Formation of magnetic clusters in the strongly frustrated hollandite vanadium oxide $V_{7.22}O_8(OH)_8Cl_{0.77}(H_3O)_{2.34}$

Natasha A. Chernova,* J. Katana Ngala,† Peter Y. Zavalij,‡ and M. Stanley Whittingham
Institute for Materials Research, State University of New York at Binghamton, Binghamton, New York 13902-6000, USA
(Received 5 May 2005; revised manuscript received 29 August 2006; published 2 January 2007)

Magnetic properties of the first hollandite-type vanadium oxide containing anions in the 2×2 channels, $V_{7.22}O_8(OH)_8(Cl)_{0.77}(H_3O)_{2.34}$, are studied via static (dc) and dynamic (ac) magnetic susceptibilities and heat capacity. At 25 K a rapid increase of magnetic susceptibility is observed; the field-cooled and zero-field-cooled susceptibilities diverge below this temperature and magnetization shows a pronounced hysteresis. The temperature dependence of dc susceptibility follows the Curie-Weiss law above 350 K; the effective magnetic moment per vanadium ion is consistent with the 3+ oxidation state. The negative Curie-Weiss temperature $\Theta\approx-336$ K indicates strong antiferromagnetic exchange; combined with low transition temperature, this reveals significant spin frustration. The real χ' and imaginary χ'' components of the ac susceptibility show two frequency-dependent maxima at 17.5 and 7 K that shift toward lower temperatures with decreasing frequency. The temperature dependences of the spin relaxation time τ in various magnetic fields H were obtained by the Cole-Cole method and analyzed using the scaling law. A very slow relaxation with characteristic times of the order of 10^{-3} s was found, consistent with fluctuation of cluster magnetic moments. Temperature dependence of the specific heat does not reveal long-range magnetic order down to 2 K. Magnetic specific heat shows a broad maximum centered at 25 K, which is consistent with formation and blocking of cluster magnetic moments. Magnetic exchange pathways in the hollandite structure are analyzed, and a mechanism of magnetic cluster formation is proposed.

DOI: 10.1103/PhysRevB.75.014402 PACS number(s): 75.50.Lk, 75.40.Cx, 75.40.Gb, 75.50.Ee

I. INTRODUCTION

Vanadium oxide compounds show a great variety of interesting electronic and magnetic properties such as insulator-metal transitions in binary vanadium oxides[1,2] and low-dimensional magnetism in the intercalated layered oxides with V_2O_5, V_4O_{10}, V_3O_7, and other types of layers.[3–8] In these oxides vanadium has different types of oxygen coordination: octahedral, tetrahedral, and square pyramidal, with the oxidation state varying from 3+ to 5+.[9] The hollandite-type vanadium oxides stand apart from the layered ones. The hollandite structure contains tunnels built of double chains of edge-sharing MO_6 octahedra (here M is usually a transition metal, for example, Mn in the original hollandite MnO_2, or V, Fe, Ni, Mo, etc.).[10] The channels are most often occupied by alkaline, alkaline earth, or other metal cations (Fig. 1). Hollandite-type compounds possess interesting magnetic and electrical properties due to one or more of the following factors: quasi-one-dimensional (1D) character of the tunnel walls, mixed valence of the transition metal, and partial occupancy of tunnels or MO_6 octahedra. $Bi_xV_8O_{16}$ ($1.72<x<1.8$) shows a temperature-induced metal-insulator transition accompanied by a strong increase of the magnetic susceptibility, which is explained by a charge and orbital ordering being possible as the V^{3+}/V^{4+} ratio is getting close to 2/1.[11,12] $K_{1.5}(H_3O)_xMn_8O_{16}$ ($0<x<0.5$) shows three magnetic phase transitions that are sensitive to the amount of H_3O^+ ions, causing the possibility of Mn^{3+}/Mn^{4+} ordering.[13] $BaRu_6O_{12}$ shows one-dimensional electronic properties and a quantum phase transition sensitive to disorder.[14]

We have synthesized a hollandite compound, $V_{7.22}O_8(OH)_8(Cl)_{0.77}(H_3O)_{2.34}$, the first one containing anions in the tunnels (Fig. 1). It has occupational disorder at the vanadium sites as well as in the tunnels, while the vanadium is believed to be mostly in a single oxidation state V^{3+}.[15,16] In this paper we discuss the magnetic properties of this compound. The rest of the paper is organized as follows. In Sec. II, the experimental setup and procedures are introduced. In Sec. III A, the static magnetic properties of the hollandite compound are presented including temperature and magnetic field dependences of magnetization and irreversible behavior in the low-temperature phase. Section III B describes the dynamic susceptibility of the compound under variation of the ac field frequency and coapplied dc field. The temperature dependences of characteristic relaxation times are determined and analyzed. Section III C covers the results of the specific heat measurements, revealing that no long-range order is established in the hollandite compound down to 2 K. In Sec. IV, the obtained results are discussed using the model of magnetic clusters formation and a subsequent cluster-glass transition. The crystal structure is examined to reveal magnetic exchange pathways and the origin of the magnetic cluster formation. Section V concludes the paper summarizing the main results obtained.

II. EXPERIMENT

The hollandite compound

$$V_{7.22(4)}O_8(OH)_8(Cl)_{0.77(2)}(H_3O)_{2.34(8)}$$

was synthesized hydrothermally and characterized by TGA using a Perkin Elmer model TGA 7, scanning electron microscopy and EDS on a JEOL 8900, and FTIR using a Bruker EQUINOX 55 instrument. The structure of the compound was determined from x-ray powder diffraction data

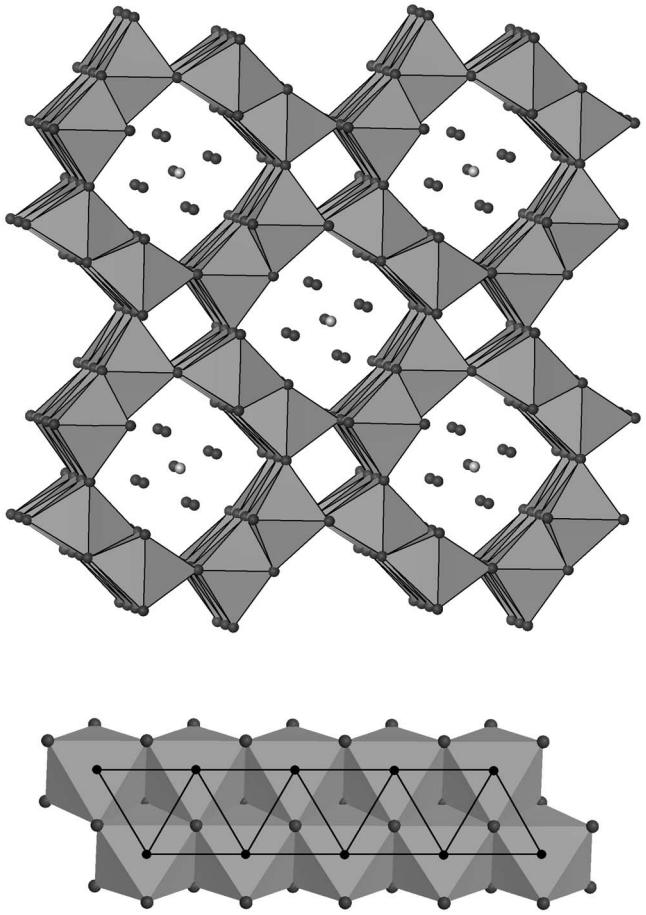

FIG. 1. Crystal structure of $V_{7.22}O_8(OH)_8(Cl)_{0.77}(H_3O)_{2.34}$ viewed along c axis (top). Vanadium ions occupy VO_6 octahedra, which share edges to form double chains. A double chain structure is presented at the bottom; triangular motif of vanadium ions is shown. Four chains share corners to form tunnels occupied by chlorine (light circles) and hydroxonium (dark circles, hydrogen atoms are omitted for clarity) ions.

obtained using Cu $K\alpha$ radiation on a Scintag θ-θ XDS2000 diffractometer equipped with a Ge(Li) solid state detector. The details of the synthesis and structural characterization may be found in Ref. 15.

The magnetic properties were studied on a powder sample, mass 0.1 g, using a Quantum Design SQUID magnetometer (MPMS XL-5). The temperature dependence of the dc susceptibility ($\chi=M/H$, where M is the magnetization of the sample and H is the applied constant magnetic field) was measured while cooling the sample from 400 down to 2 K in a magnetic field of 1000 Oe. Field-cooled (FC) and zero-field-cooled (ZFC) susceptibilities were measured from 50 to 2 K in magnetic fields from 10 to 5000 Oe. FC susceptibility was measured by cooling the sample in the magnetic field; before taking ZFC data, the remanent magnetic field was quenched below 3 mOe, the sample was cooled down to 2 K, then the magnetic field was applied and the temperature dependence was measured while heating the sample. The temperature dependences of the ac susceptibility were measured in the ac field $h=4$ Oe at various frequencies f from 0.05 to 1000 Hz, coapplied dc field was varied from

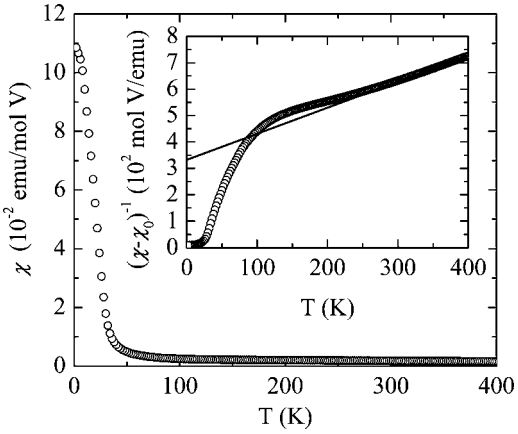

FIG. 2. Temperature dependence of magnetic susceptibility $\chi=M/H$ measured in dc field $H=1000$ Oe. Inset shows reciprocal susceptibility corrected due to temperature-independent contribution ($\chi_0=2.2\times10^{-4}$ emu/mol V). The straight line is the best fit to the Curie-Weiss law at high temperatures.

0 to 1000 Oe. The sample was zero-field cooled as described above and the ac data were collected while heating the sample.

For the resistivity measurements, the material was hot pressed into a pellet whose resisitivity was measured using the two-probe method in the temperature range from 300 to 140 K. The heat capacity of the pressed pellet was measured using Quantum Design Physical Properties Measurement System in the temperature range 2 to 350 K.

III. EXPERIMENTAL RESULTS AND ANALYSIS

A. Static magnetic properties

The dc magnetic susceptibility χ measured as a function of temperature rapidly increases around 25 K indicating a magnetic phase transition (Fig. 2). The transition temperature determined as minimum of $d\chi/dT$ is $T_c\approx19.5$ K. The $\chi(T)$ dependence does not follow the Curie-Weiss law for up to room temperature indicating a strong magnetic exchange which probably leads to a short-range magnetic order. The fit to the Curie-Weiss law $\chi=\chi_0+C/(T-\Theta)$ above 350 K (straight line in Fig. 2 inset) produces very reasonable parameters: the temperature-independent contribution $\chi_0=(2.2\pm0.1)\times10^{-4}$ emu/mol V, the Curie constant $C=0.99\pm0.03$ emu K/mol V, and the asymptotic Curie-Weiss temperature $\Theta=-336\pm1$ K. The determined value of the Curie constant corresponds to the effective magnetic moment of 2.84 μ_B per vanadium, consistent with the 3+ oxidation state. The high and positive temperature-independent susceptibility may be attributed to the Van-Vleck contribution. The negative sign and the high absolute value of Θ indicate strong antiferromagnetic exchange between the vanadium ions, which explains a deviation from the Curie-Weiss paramagnetic behavior at low temperatures. The absolute value of Θ is more than 15 times larger than T_c, revealing a strong spin frustration.

In the low-temperature phase, the temperature dependences of magnetization measured under the ZFC conditions

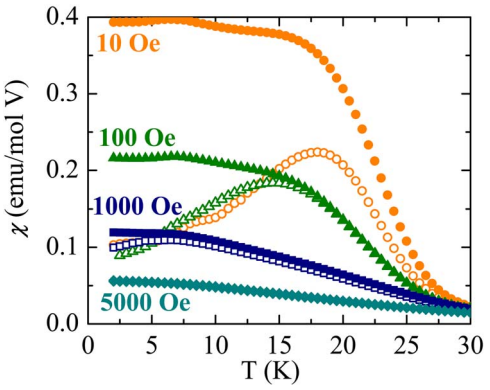

FIG. 3. (Color online) Field-cooled (solid symbols) and zero-field cooled (open symbols) dc magnetizations versus temperature measured for various magnetic fields.

deviate from those measured under the FC conditions (Fig. 3). In small fields, $H \leqslant 100$ Oe, the FC and ZFC curves reveal an additional small maximum around 7 K, which might indicate a second phase transition. Increasing H rapidly suppresses the amplitude of the large high-temperature ZFC maximum and makes it shift toward lower temperatures. The irreversibility temperature decreases with H, as does the difference between FC and ZFC curves. At and above 5000 Oe no difference between FC and ZFC susceptibilities is found. The shape of the FC and ZFC curves around the phase transition is not typical for spin glasses and rather indicates that the FC-ZFC difference originates from the net magnetic moment formation, which is also evident from the hysteresis of magnetization (Fig. 4) found below T_c.

B. Dynamic ac susceptibility

The temperature dependences of the ac susceptibility in the absence of the dc field are presented in Fig. 5. Both the dispersion χ' and absorption χ'' show two frequency-dependent maxima around 17.5 and 7 K. With the decreasing frequency the magnitude of the dispersion peaks increases, and they shift slightly towards lower temperatures. The magnitude of the absorption peak at 17.5 K also decreases with decreasing frequency, while the intensity of the small peak at 7 K increases. The shift towards lower frequency is more

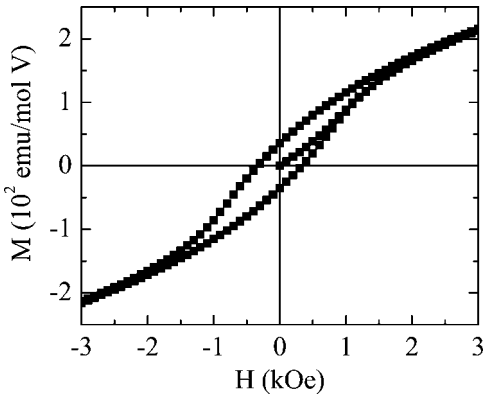

FIG. 4. Magnetization as a function of applied field at 2 K.

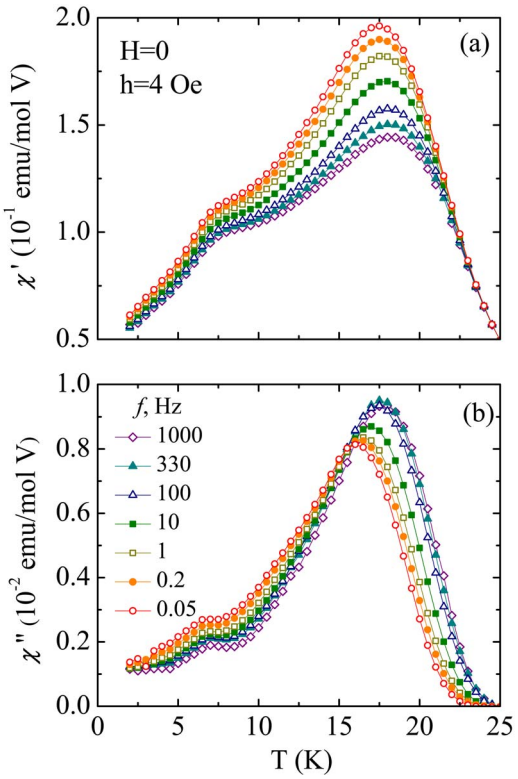

FIG. 5. (Color online) Temperature dependences of real (a) and imaginary (b) components of ac susceptibility measured with ac field of amplitude $h=4$ Oe at various frequencies.

pronounced for the absorption peaks. The relative shift of the high-temperature absorption maximum per decade of angular frequency $\omega=2\pi f$ is $\Delta T_c/[T_c \Delta(\ln \omega)] \approx 0.02$ which is close to the values found in spin glasses and spin-glass like systems with short-range magnetic interactions.[17]

With increasing dc magnetic field the amplitude of the high-temperature peak decreases for both χ' and χ''; the peaks shift towards lower temperatures, so that at and above 500 Oe only one peak is observed (Fig. 6). The amplitude of the low-temperature peak increases slightly in small fields, but above 100 Oe a steady decrease is observed. This peak also shifts to lower temperature when H is increased. The observed decrease of the susceptibility indicates that coapplied dc magnetic field suppresses spin fluctuations, while the peak shift towards lower temperatures is consistent with the antiferromagnetic exchange. The nature of the second peak and the initial increase of its amplitude with H remain unclear, and the spin processes taking place around the high-temperature susceptibility maximum also require clarifications. Temperature dependences of the relaxation time τ around T_c in both zero magnetic field and in the applied dc field could have helped to understand these phenomena.

The temperature dependence of the relaxation time τ may be obtained from the frequency dependence of χ' and χ'' using the Cole-Cole method. This analysis is based on the assumption that the distribution of relaxation times is symmetrical on a logarithmic scale.[18] Then

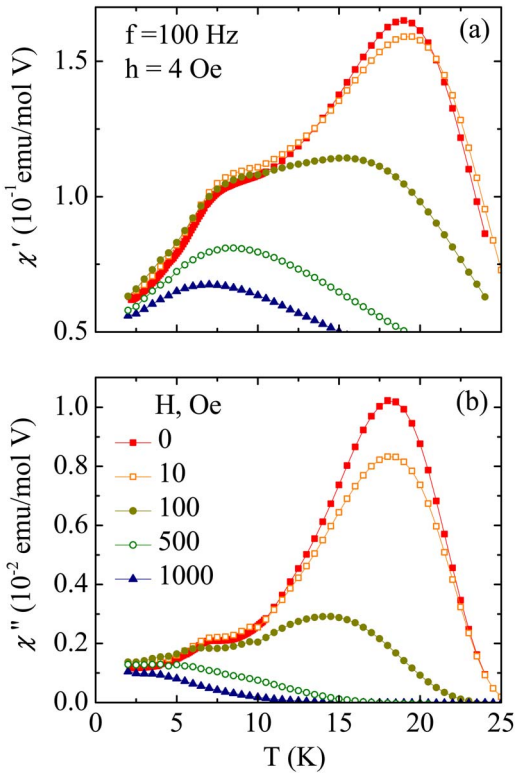

FIG. 6. (Color online) Temperature dependences of real (a) and imaginary (b) components of ac susceptibility measured with ac field of amplitude $h=4$ Oe and frequency $f=100$ Hz in various dc fields H.

$$\chi(\omega) = \chi_S + \frac{\chi_0 - \chi_S}{1 + (i\omega\tau_c)^{1-\alpha}}, \tag{1}$$

where χ_0 and χ_S are the isothermal and adiabatic susceptibilities, respectively, and τ_c is the median relaxation time. The parameter α determines the width of the distribution: $\alpha=1$ corresponds to an infinitely wide distribution, while $\alpha=0$ corresponds to the case of a single relaxation time. Equation (1) may be decomposed into the frequency dependences of real and imaginary susceptibilities as

$$\chi'(\omega) = \chi_S + \frac{\chi_0 - \chi_S}{2} \times \left[1 - \frac{\sinh[(1-\alpha)\ln(\omega\tau_c)]}{\cosh[(1-\alpha)\ln(\omega\tau_c)] + \sin(1/2\alpha\pi)}\right], \tag{2}$$

$$\chi''(\omega) = \frac{\chi_0 - \chi_S}{2}\left[\frac{\cos(1/2\alpha\pi)}{\cosh[(1-\alpha)\ln(\omega\tau_c)] + \sin(1/2\alpha\pi)}\right]. \tag{3}$$

Equations (2) and (3) can be used directly to fit the experimental data; however, it is more reliable to eliminate τ_c from these equations and to start with the fitting of $\chi''(\chi')$ dependences in a complex plane with three variables, χ_0, χ_S, and α

$$\chi''(\chi') = -\frac{\chi_0 - \chi_S}{2\tan[1/2\pi(1-\alpha)]} + \left[\left(\frac{\chi_0 - \chi_S}{2}\right)^2 - \left(\frac{\chi_0 - \chi_S}{2\tan[1/2\pi(1-\alpha)]}\right)^2 - \left(\chi' - \frac{\chi_0 + \chi_S}{2}\right)^2\right]^{1/2}. \tag{4}$$

According to this theory, the $\chi''(\chi')$ curves are arcs with the length $(1-\alpha)\pi(\chi_0-\chi_S)$, intersecting the abscissa at $\chi'=\chi_S$ and $\chi'=\chi_0$. At the maximum of χ'', $\omega\tau_c=1$. The experimental $\chi''(\chi')$ look like superposition of several arcs (from 1 to 4 at different temperatures, but at most temperatures as 3 arcs) that reflect a presence of several relaxation processes. However most of the arcs are too small to be accurately analyzed, therefore we will analyze only the low-frequency arc of $\chi''(\chi')$ curves from 1 to 0.05 Hz as they are the longest ones and experience the most change when the temperature is lowered through the phase transition. As seen from Fig. 7, the model shows excellent fit to the experimental data. The experimental $\chi''(\chi')$ data [Fig. 7(a)] go through the maximum towards the adiabatic limit when the temperature is lowered beyond the T_c. This indicates a significant increase of the relaxation time around the phase transition. The temperature dependences of the relaxation times are presented in Fig. 8 for increasing values of the magnetic field H. The $\tau(T)$ dependences for nonzero H were obtained in the same manner as above.

In zero field H the relaxation time increases by more than 3 orders of magnitude when the temperature is lowered through the phase transition. With increasing H the dependences shift towards lower temperatures, and the range of the relaxation times decreases as the fast relaxation times can no longer be obtained. This happens because the transition temperature lowers with the magnetic field while the following limitations exist for the determination of τ using the Cole-Cole method: at high temperatures χ_S tends to zero, χ_0 also decreases and the $\chi''(\chi')$ arc collapses, while at low temperatures χ_0 and τ go to infinity and the fit diverges.

The $\tau(T)$ dependences were analyzed using the scaling law $\tau=\tau_0(T/T_c-1)^{-z\nu}$ which produces a good fit for all magnetic fields (solid lines in Fig. 8). The values of the characteristic relaxation time τ_0, critical temperature T_c, and dynamical critical exponent $z\nu$ are summarized in Table I. At zero H, the characteristic relaxation time is almost 10^{-3} s, T_c is about 11 K, and $z\nu$ is 8. The characteristic relaxation time is extremely long, while the critical exponent $z\nu$ falls in the range 8–12 that is usually observed in spin glasses.[17] The similarity of $z\nu$ values indicates that the spin dynamics in the hollandite compound is close to that of spin glasses. However, longer relaxation times correspond to the blocking of cluster magnetic moments as opposed to the freezing of individual spins found in spin glasses.

C. Specific heat

We have studied the heat capacity of the vanadium hollandite compound in order to check whether the 7 K susceptibility maximum corresponds to a long-range magnetic ordering transition. The temperature dependence of the

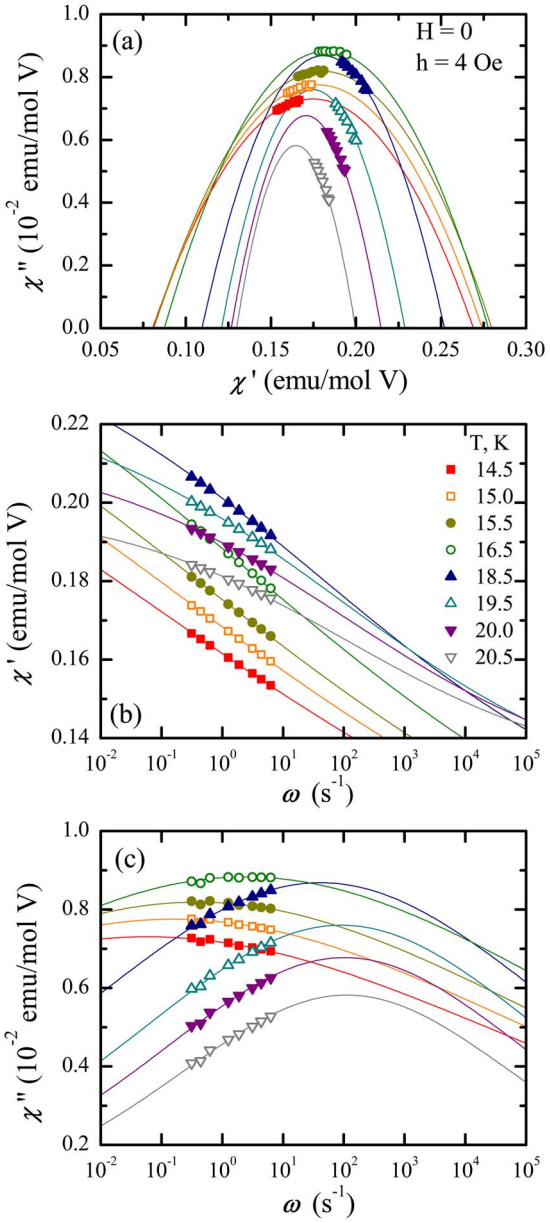

FIG. 7. (Color online) Argand plots (a) and frequency dependences of real (b) and imaginary (c) components of ac susceptibility for low-frequency relaxation process, $0.05 \leqslant f \leqslant 1$ Hz. Solid lines are the best fits to the Cole-Cole model, Eqs. (2)–(4).

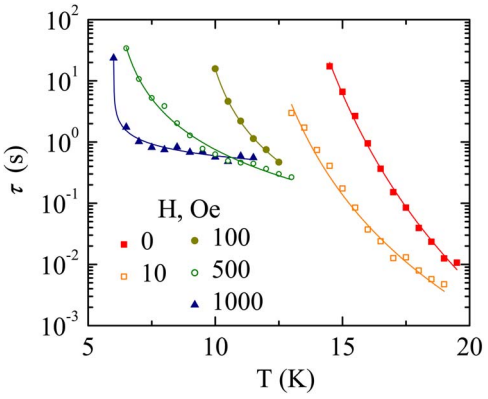

FIG. 8. (Color online) Temperature dependences of characteristic relaxation time determined for various dc fields H for low-frequency relaxation process. Solid lines are the best fits to the scaling law.

specific heat (Fig. 9) does not show any features at either of the two susceptibility maxima temperatures, meaning that the long-range magnetic order is not established in the hollandite compound down to 2 K. A very general expression $C_p = \gamma T + \beta T^3 + BT^n$ was used to check the contributions to the specific heat in the hollandite compound (the fit is shown as a solid line in Fig. 9). The first, linear term is related to the heat capacity of conduction electrons; this term is absent in the hollandite compound, $\gamma = 0$. This is consistent with high resistivity following the Arrhenius type temperature dependence (Fig. 10). Phonon contribution is described by the T^3 term with the coefficient $\beta = 0.65 \pm 0.05$ mJ/mol K^4 which corresponds to the Debye temperature $\theta_D = 430 \pm 10$ K (the error comes mostly from the different choices of temperature interval for the fitting). This result is consistent with θ_D of 420 to 460 K reported for titanium hollandite with Cs ions in the tunnels.[19] The last term corresponds to the magnetic specific heat. The exponent n varies from 1.5 to 1.8 for various temperature intervals up to 40 K; the coefficient B is quite large, 0.45 ± 0.20 J/mol K$^{5/2}$. The n values are surprisingly close to that of ferromagnetic magnons, $n = 3/2$. The ferromagnetic magnons may exist in a magnetically ordered compound in the presence of net magnetic moment. As we have established, the low-temperature phase possesses a net magnetic moment but there is no long-range magnetic order. On the other hand, the magnetic order may be established within clusters; if the cluster size is large enough, the ferromagnetic magnons could still be observed. The large value of B indicates that the spin-wave stiffness constant is small, $D = 7 \pm 3$ meV Å^2, which is consistent with the presence of vanadium vacancies leading to reduced magnetic exchange and softer spin waves. It should be pointed out that it is quite unusual to find a power-law contribution with the exponent close to 3/2 for the heat capacity of a nonferromagnetic compound. The attempts to fix n at other values, for example, $n = 2$ typical for two-dimensional (2D) antiferromagnets, produce only a poor fit.

We have separated the magnetic part of the specific heat by subtracting the lattice contribution (Fig. 11). The latter was estimated from the specific heat of structurally similar nonconductive and nonmagnetic compounds: rutile

TABLE I. Characteristic relaxation times, critical temperatures, and dynamical critical exponents for the slowest spin relaxation processes for various magnetic fields derived from the fit of the temperature dependences of relaxation time to the scaling law.

H [Oe]	τ_0 [s]	T_c [K]	$z\nu$
0	$6.4(1) \times 10^{-4}$	11.0(8)	8(1)
10	$1.0(4) \times 10^{-3}$	10.6(9)	6(2)
100	$3.9(1) \times 10^{-2}$	9.2(1)	2.5(2)
500	$3.7(3) \times 10^{-1}$	5.8(1)	2.1(2)
1000	$5.0(3) \times 10^{-1}$	6.0(1)	0.45(5)

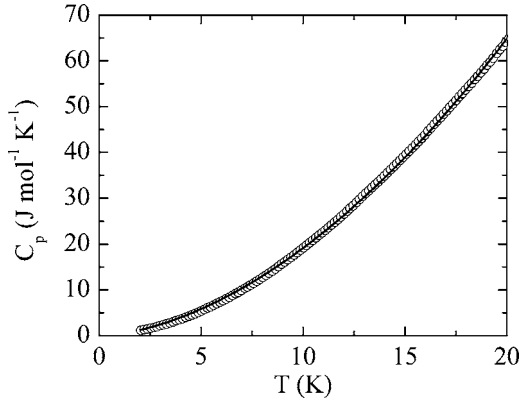

FIG. 9. Temperature dependence of specific heat (scattered data). Solid line represents a theoretical fit (see text for details).

TiO_2 (Ref. 20) and β-eucryptite $LiAlSiO_4$ which is claimed to have the same heat capacity as hollandite $K_{2x}Mg_xTi_{8-x}O_{16}$.[21,22] The specific heat data of the above model compounds are presented in Fig. 11(a) together with the approximation obtained from the polynomial fit (solid line). The latter was subtracted from the specific heat of the vanadium hollandite. The resulting magnetic specific heat [Fig. 11(b)] shows a broad peak with an onset above 75 K, around the same temperature when the magnetic susceptibility starts to significantly diverge from the Curie-Weiss law. This confirms appearance of the short-range magnetic correlations well above the transition temperature. The magnetic entropy at 75 K estimated using equation

$$S_m(T) = \int_0^T \frac{C_m(T)}{T} dT \tag{5}$$

is about 9.5 J/(mol V K), close to the theoretical value for the spin degree of freedom $S_m = R\ln(2S+1) = 9.13$ J/(mol V K) for $S=1$ V^{3+} ions [Fig. 11(c)]. At $T=17.5$ K magnetic entropy is only about 1/3 of the theoretical value, and at 7 K a negligible magnetic entropy remains. The magnetic heat capacity peak is wide, centered at about 25 K, i.e., at the same temperature range where the most rapid increase of magnetization is found. These data agree well with the gradual formation of magnetic clusters of various sizes followed by the transition to a cluster-glass magnetic phase. The true transition temperature is not clear from the heat capacity data; different magnetic measurements also provide different T_c values. The best estimation is, probably, the one obtained from the scaling analysis of the $\tau(T)$ dependence, $T_c = 11.0(8)$ K, which means that at 11 K cluster magnetic moments are frozen. The nature of the 7 K magnetic susceptibility anomaly was not revealed by the heat capacity studies; therefore it should be a minor magnetic moment rearrangement easily suppressed by an applied magnetic field.

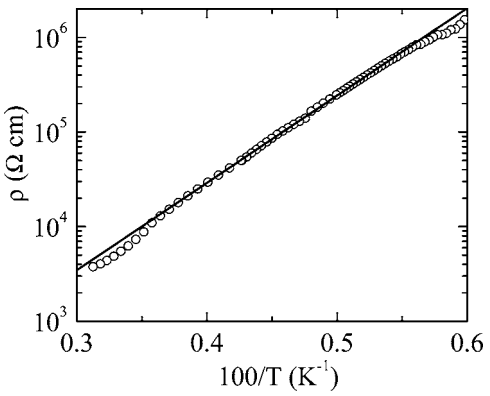

FIG. 10. Resistivity as a function of temperature and its fit to Arrhenius-type dependence.

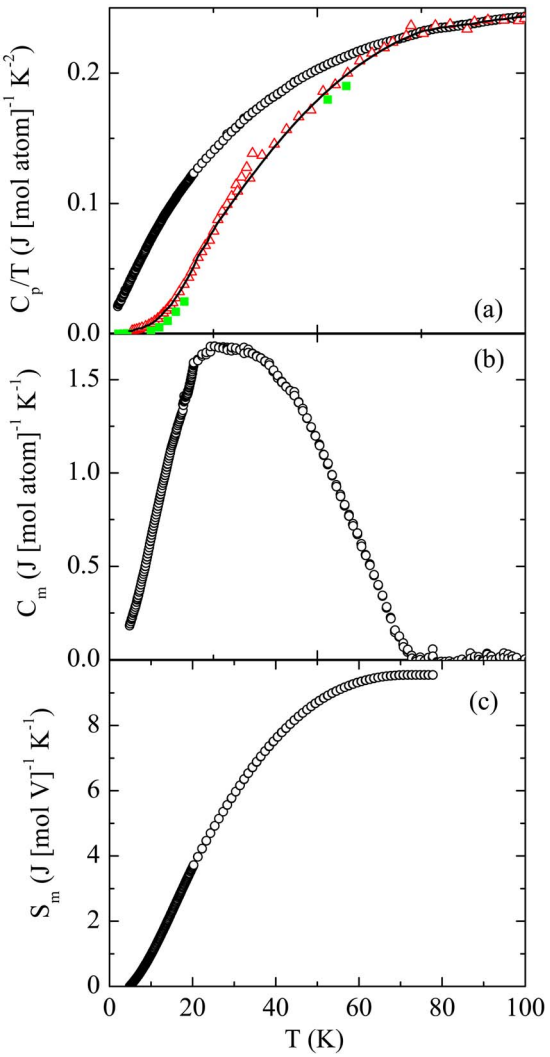

FIG. 11. (Color online) (a) C_p/T as a function of temperature for the hollandite $V_{7.22}O_8(OH)_8(Cl)_{0.77}(H_3O)_{2.34}$ (open circles) and nonmagnetic structurally similar compounds used to estimate lattice specific heat. Data for rutile TiO_2 is shown in solid squares, and for β-eucryptite $LiAlSiO_4$ (known to have the same heat capacity as hollandite $K_{2x}Mg_xTi_{8-x}O_{16}$) is shown as open triangles. Solid line is a polynomial approximation over the latter two data sets representing lattice contribution to the specific heat. (b) Magnetic specific heat of $V_{7.22}O_8(OH)_8(Cl)_{0.77}(H_3O)_{2.34}$ obtained by subtraction of lattice contribution from C_p. (c) Temperature dependence of magnetic entropy.

IV. DISCUSSION

The vanadium hollandite compound with chloride and hydroxonium ions in the channels shows a cluster-glass behavior which is different from the magnetic properties of vanadium hollandites with bismuth, lead, potassium, and other ions.[11,23–25] There are several structurally related reasons to explain this difference. In the considered compound all the vanadium ions have the same oxidation state +3, and the compound is not conducting with a room-temperature resistivity of $2\times10^3\ \Omega\,\mathrm{cm}$. Similar behavior was found in mixed-valence $K_xBi_yV_8O_{16}$ hollandite which shows Arrhenius behavior due to hopping semiconduction.[26] However, in mixed-valence $Bi_xV_8O_{16}$ hollandites high values of conductivity and Pauli paramagnetism at room temperature are reported,[11,24,25] indicating high carrier concentration in the partially occupied conduction band. None of these mechanisms is our case, and we can assume that in this compound the *d*-band splitting occurs in such a way that the lowest subband is fully occupied for the d^2 V^{3+} case. As for the magnetic properties, the absence of electronic conductivity means the presence of localized magnetic moments, as opposed to Pauli paramagnetism of bismuth hollandites.

The localized magnetic moments experience strong exchange in the hollandite structure. The tunnel walls are built of the double chains of edge-sharing VO_6 octahedra (Fig. 1), thus there is a direct overlap of the t_{2g} orbitals providing strong antiferromagnetic exchange. On the other hand, all antiferromagnetic interactions cannot be satisfied simultaneously in the double chains, where the vanadium ions are arranged in triangular motif (bottom part of Fig. 1), therefore very strong spin frustration occurs, evidenced experimentally. The four double-chain walls are connected by corner sharing to form tunnels. The magnetic moments in the corner-sharing VO_6 octahedra may interact by 180° superexchange. Though this interaction is weak for the d^2-d^2 case, apparently it is strong enough to provide three-dimensional magnetic exchange. As we remember, no signs of one-dimensional magnetism were found experimentally.

The other important structural feature is the presence of about 10% of disordered vacancies in the vanadium sublattice. It is interesting to note that the concentration of chloride ions is roughly equal to the concentration of vanadium vacancies. Randomly distributed vacancies facilitate formation of the vanadium clusters of various sizes, which can also be considered as magnetic domains. Upon temperature decrease the vanadium magnetic moments order within the cluster, net magnetic moment increases, and ferromagnetic phonons may be observed. The exact type of antiferromagnetic order cannot be determined at this point, but magnetic moment formation rules out a simple collinear antiferromagnetic order.

V. CONCLUSION

The hollandite-type vanadium oxide $V_{7.22}O_8(OH)_8(Cl)_{0.77}(H_3O)_{2.34}$ with single V^{3+} oxidation state reveals a strong antiferromagnetic exchange between V^{3+} spins in edge-sharing octahedra. Geometric frustration prevents a long-range magnetic ordering which does not occur down to 2 K as evidenced by heat capacity measurements. The increase of magnetic moment observed around 25 K in dc magnetization and slow relaxation processes (characteristic time of the order of 10^{-3} s) found using ac susceptibility are explained by magnetic cluster formation and blocking of cluster magnetic moments. A $T^{3/2}$ term was found in the specific heat of the compound and ascribed to very soft ferromagnetic magnons existing within clusters. Magnetic cluster formation in the compound is explained by partial (90%) occupation of the vanadium sites.

ACKNOWLEDGMENTS

This work was supported by the National Science Foundation through Grant No. DMR 0313963. We thank Jim O'Brien from Quantum Design for the heat capacity measurements.

*Electronic address: chernova@binghamton.edu
†Present address: Department of Chemistry, University of Connecticut, Storrs, CT 06269.
‡Present address: Department of Chemistry and Biochemistry, University of Maryland, College Park, MD 20742.

[1] N. F. Mott, *Metal-Indulator Transitions* (Taylor & Francis, London, 1974).
[2] M. Imada, A. Fujimori, and Y. Tokura, Rev. Mod. Phys. **70**, 1039 (1998).
[3] Y. Ueda, Chem. Mater. **10**, 2653 (1998).
[4] M. Onoda and R. Arai, J. Phys.: Condens. Matter **13**, 10399 (2001).
[5] M. Onoda and J. Hasegawa, J. Phys.: Condens. Matter **14**, 5045 (2002).
[6] M. Kanada, H. Harashina, S. Tanaka, T. Fukamachi, Y. Kobayashi, and M. Sato, J. Phys. Soc. Jpn. **67**, 2904 (1998).
[7] S. T. Lutta, N. A. Chernova, P. Y. Zavalij, and M. S. Whittingham, J. Mater. Chem. **14**, 2922 (2004).
[8] S. Taniguchi, T. Nishikawa, Y. Yasui, Y. Kobayashi, M. Sato, T. Nishioka, M. Kontani, and K. Sano, J. Phys. Soc. Jpn. **64**, 2758 (1995).
[9] P. Y. Zavalij and M. S. Whittingham, Acta Crystallogr., Sect. B: Struct. Sci. **B55**, 627 (1999).
[10] F. Gronvold, H. Haraldsen, B. Pedersen, and T. Tufte, Rev. Chim. Miner. **6**, 215 (1969).
[11] H. Kato, T. Waki, M. Kato, K. Yoshimura, and K. Kosuge, J. Phys. Soc. Jpn. **70**, 325 (2001).
[12] Y. Shibata and Y. Ohta, J. Phys. Soc. Jpn. **71**, 513 (2002).
[13] H. Sato, T. Enoki, J.-I. Yamaura, and N. Yamamoto, Phys. Rev. B **59**, 12836 (1999).
[14] Z. Q. Mao, T. He, M. M. Rosario, K. D. Nelson, D. Okuno, B. Ueland, I. G. Deac, P. Schiffer, Y. Liu, and R. J. Cava, Phys. Rev. Lett. **90**, 186601 (2003).
[15] J. K. Ngala, N. A. Chernova, P. Y. Zavalij, and M. S. Whittingham, J. Solid State Chem. (to be published).
[16] N. A. Chernova, J. K. Ngala, P. Y. Zavalij, and M. S. Whitting-

ham, Mater. Res. Soc. Symp. Proc. **848**, 262 (2005).
[17] J. A. Mydosh, *Spin Glasses: An Experimental Introduction* (Taylor & Francis, London, 1993).
[18] K. S. Cole and R. H. Cole, J. Chem. Phys. **9**, 341 (1941).
[19] R. W. Cheary, Acta Crystallogr., Sect. B: Struct. Sci. **47**, 325 (1991).
[20] Y. S. Touloukian and E. H. Buyco, *Specific Heat: Nonmetallic Solids* (IFI/Plenum, New York, 1970).
[21] E. Gmelin and R. Villar, Physica B & C **108**, 1003 (1981).
[22] E. Gmelin, Thermochim. Acta **399**, 241 (2003).
[23] H. Okada, N. Kinomura, S. Kume, and M. Koizumi, Mater. Res. Bull. **13**, 1047 (1978).
[24] P. A. Ramakrishnan, M. Sugantha, U. V. Varadaraju, and T. Nagarajan, Mater. Lett. **36**, 137 (1998).
[25] T. Waki, H. Kato, M. Kato, and K. Yoshimura, J. Phys. Chem. Solids **63**, 961 (2002).
[26] O. Mentre, A.-C. Dhaussy, and F. Abraham, J. Mater. Chem. **9**, 1023 (1999).